Electronic transport anisotropy of 2D carriers in biaxial compressive strained germanium

C. Morrison, and M. Myronov

Citation: Appl. Phys. Lett. **111**, 192103 (2017);
View online: https://doi.org/10.1063/1.5010933
View Table of Contents: http://aip.scitation.org/toc/apl/111/19
Published by the American Institute of Physics

Electronic transport anisotropy of 2D carriers in biaxial compressive strained germanium

C. Morrison and M. Myronov
Department of Physics, University of Warwick, Coventry CV4 7AL, United Kingdom

(Received 23 April 2017; accepted 27 October 2017; published online 8 November 2017)

The anisotropic nature of carrier mobility in simple cubic crystalline semiconductors, such as technologically important silicon and germanium, is well understood as a consequence of effective mass anisotropy arising from a change in band structure along non-identical surface crystal directions. In contrast to this, we show experimentally that this type of anisotropy is not the dominant contribution. Recent advances in epitaxial growth of high quality germanium enabled the appearance of high mobility 2D carriers suitable for such an experiment. A strong anisotropy of 2D carrier mobility, effective mass, quantum, and transport lifetime has been observed, through measurements of quantum phenomena at low temperatures, between the ⟨110⟩ and ⟨100⟩ in-plane crystallographic directions. These results have important consequences for electronic devices and sensor designs and suggest similar effects could be observed in technologically relevant and emerging materials such as SiGe, SiC, GeSn, GeSnSi, and C (Diamond). https://doi.org/10.1063/1.5010933

For any electronic or spintronic device applications, it is important to understand the effect of crystallographic direction on the transport properties of the quantum well (QW). Intuitively, we would expect that the carrier mobility will change upon changing between non-identical crystallographic orientations, for example, a rotation of 45° on a (001) orientation wafer between ⟨110⟩ and ⟨100⟩ directions. This is due to the change in band structure and consequently a change in the effective mass of the carriers. However, we must also consider the effect of scattering mechanisms such as interface and impurity scattering, which may also depend on the direction of carrier flow in the plane of the wafer. For example, silicon and germanium have the same lattice structure. It is very well known that surface orientation causes carrier mobility anisotropy in Si, and due to this, the correct selection of device surface orientation can lead to a significant performance enhancement.[1] Anisotropy of mobility in simple cubic semiconductors was first studied over 50 years ago,[2–5] and experimentally observed for electrons in Ge,[6] usually attributed to variations in band structure and consequently effective mass along non-equivalent crystallographic orientations. A previous study of p-type Ge-on-insulator (GOI) channels has shown significant mobility anisotropy when the channel is oriented along the ⟨100⟩ or ⟨110⟩ directions, due to effective mass anisotropy.[7] It is another example where both electron and holes mobility surface orientation anisotropy in Si or Ge are simply explained by differences in effective mass. In contrast to this work, we experimentally show it is not the case for 2D holes in compressively strained Ge. Our recent study of a series of square devices containing Ge QW heterostructures concluded that wafer axis tilt resulted in significant 2D hole gas (2DHG) mobility anisotropy between nominally identical ⟨110⟩ directions.[8]

Strained Si, Ge, and SiGe quantum well (QW) heterostructures are a promising material system for conventional electronic, spintronic, and quantum technology device applications due to high hole mobility, tunable spin splitting, and compatibility with existing Si-based technology. SiGe has already been implemented in a large variety of modern high end electronic devices including heterojunction bipolar transistor (HBT), complementary metal oxide semiconductor (CMOS), and others to enable either a very high speed or a very low power consumption of modern portable equipment including laptops, smartphones, and smartwatches. Until fairly recently, hole mobility in a Ge quantum well (QW) was limited to around 120 000 $cm^2\ V^{-1}s^{-1}$ at low-temperatures. However, recent developments in epitaxial growth by reduced pressure chemical vapour deposition (RP-CVD) have allowed growth of strained Ge QW heterostructures with a 2D hole gas 2DHG mobility in excess of 1×10^6 cm^2/V s. Strained Ge QW grown by RP-CVD exhibit both interesting physical phenomena (Rashba spin-orbit splitting[9–11] and Fractional Quantum Hall effect[12]) and are also promising for device applications due to their high room and low temperature mobility [4500 $cm^2\ V^{-1}s^{-1}$ (Refs. 13 and 14) and 1,500,000 $cm^2\ V^{-1}s^{-1}$,[15,24] respectively].

In this work, we investigate the low temperature magnetotransport properties of a strained Ge QW modulation doped (MOD) heterostructure with no significant wafer tilt (<0.1°). We utilise a Hall bar device geometry [Fig. 1(a)] to provide a well-defined current direction, allowing us to study the anisotropy of transport behaviour within the (001) plane more accurately and without the assumptions required in previous methods and to improve our understanding of the physical mechanism underlying the phenomenon.[8]

The heterostructure studied here was epitaxially grown onto a standard orientation 100 mm diameter Si(001) substrate by RP-CVD. It is one of many Ge QW epitaxial structures exhibiting such a phenomenon. First, a 2.1 μm reverse linearly graded SiGe buffer was grown, terminating at a composition of $Si_{0.16}Ge_{0.84}$. Onto this buffer, a 17 nm Ge QW was grown, followed by a 30 nm $Si_{0.16}Ge_{0.84}$ spacer

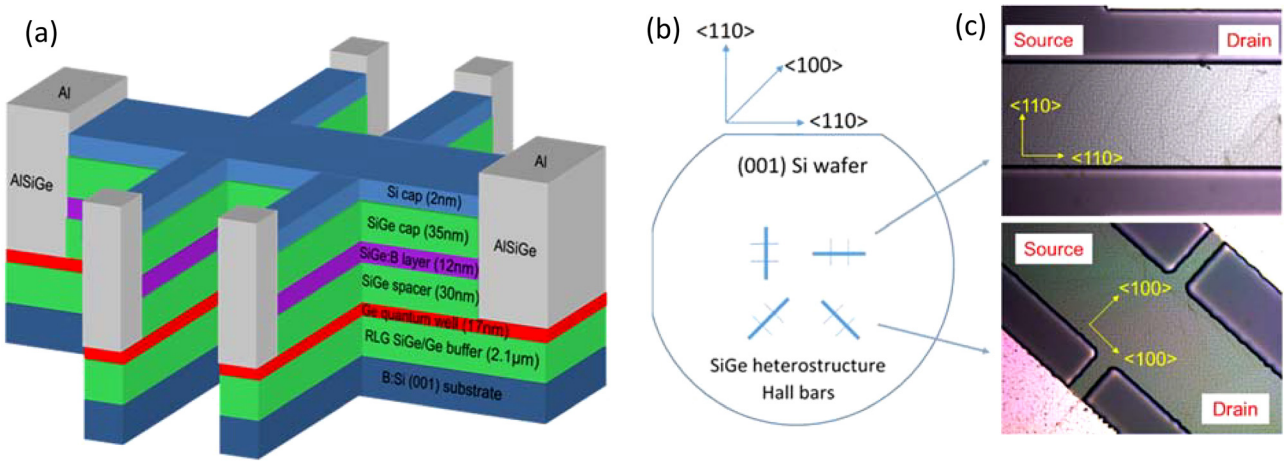

FIG. 1. (a) Schematic of the Hall bar device used, showing the composition of the heterostructure. (b) (001) plane of the wafer, illustrating the ⟨110⟩ and ⟨100⟩ directions. (c) Optical images of the Ge heterostructure Hall bars showing cross hatching from epitaxial growth. This pattern is aligned to the ⟨110⟩ directions.

layer, a 12 nm $Si_{0.16}Ge_{0.84}$ remote modulation doping layer with $\sim 2 \times 10^{18}\,cm^{-3}$ of Boron, a 35 nm $Si_{0.16}Ge_{0.84}$layer, and finally a ∼2 nm Si cap. This modulation doped structure results in a (hole) carrier density of $2.7 \times 10^{11}\,cm^{-2}$ at low temperatures, where all other layers freeze out and transport is entirely within the QW region where a 2DHG is formed.

In order to study the electrical properties of the heterostructure, a set of Hall bar devices was fabricated, with the current flow direction aligned with the ⟨110⟩ and ⟨100⟩ crystallographic directions on the wafer. The layer structure of the heterostructure is illustrated in Fig. 1(a). Figure 1(b) illustrates the orientation of the devices measured with respect to the full 100 mm wafer (not to scale). Figure 1(c) shows optical images of the central portion of the Hall bars for two orientations (⟨110⟩ and ⟨100⟩). Clear cross-hatching patterns can be seen, which develop during the epitaxial growth process of the strain relaxed graded SiGe buffer and are aligned to the ⟨110⟩ crystallographic axes. This serves to highlight the accurate alignment of the current path in the Hall bar with the wafer axes.

The electrical properties of the heterostructure were measured at temperatures between 0.3 K and 20 K using a Heliox closed cycle ^{3}He cryostat from Oxford Instruments with a superconducting magnet. The sheet carrier density falls to a constant $2.7 \times 10^{11}\,cm^{-2}$ at temperatures below ∼50 K, consistent with transport in a 2DHG formed in the QW region, as all other layers freeze out. The Hall mobility rises to a maximum of $1\,288\,000\,cm^2\,V^{-1}s^{-1}$ at ∼0.3 K for the Hall bar aligned with the ⟨110⟩ direction. The carrier density is isotropic, as highlighted in Fig. 2 which shows the Hall resistance up to 0.4 T. However, the mobility exhibits anisotropy, falling to $1\,160\,000\,cm^2\,V^{-1}s^{-1}$ along the ⟨100⟩ direction, a change of 10%. Device to device variability in mobility, measured across the 80% 100 mm wafer, is less than 0.5%. This is because the epilayer thickness uniformity and Ge content variation across our 100/150/200 mm diameter Ge QW heterostructure wafers are less than 2% and 0.1%, respectively. Variation across a few mm^2, within which the researched Hall bars were fabricated, is undetectable by HR-XRD (High Resolution X-ray diffraction), XTEM, SIMS, and AFM techniques.

In order to understand the physical origins of this 2DHG, anisotropy Shubnikov-de Haas oscillations were measured at low temperatures and the temperature dependence of these oscillations was used to determine the hole effective mass m* in the QW and the Dingle ratio relating the carrier transport lifetime to the quantum lifetime. We look for any anisotropy in these parameters as a potential explanation for the observed mobility anisotropy. Figure 3 shows magnetoresistance curves for the (a) ⟨110⟩ and (b) ⟨100⟩ directions at three temperatures between 0.33 and 0.7 K. A clear anisotropy in damping is visible between the two orientations when measured at the same temperature. Shubnikov-de Haas oscillations in the magnetoresistance of a 2DHG are described by the equation[16,17]

$$\frac{\Delta\rho_{xx}(B)}{\rho_{xx}(0)} = 4\cos\left(\frac{2\pi E_F m^*}{\hbar eB}\right)\exp\left(-\frac{\pi m^* \alpha}{eB\tau_t}\right)\frac{\psi}{\sinh(\psi)}, \quad (1)$$

where E_F is the Fermi energy, α is the Dingle ratio ($\frac{\tau_t}{\tau_q}$, where τ_t is the transport scattering time and τ_q is the quantum scattering time), and $\psi = \frac{2\pi^2 k_B T m^*}{\hbar eB}$. It therefore follows that, when considering changes in damping at a constant temperature, this may occur from changes in the effective mass, the

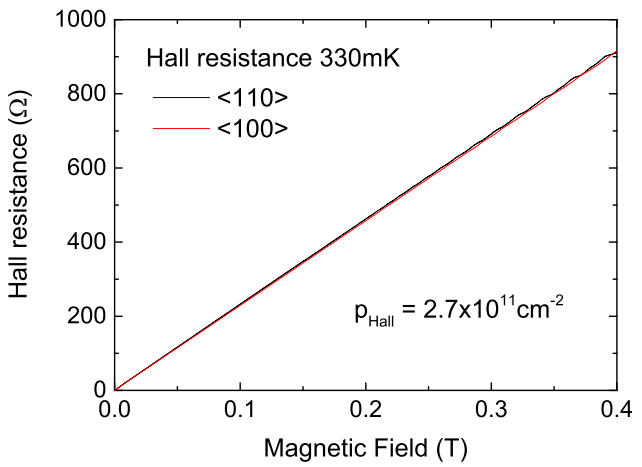

FIG. 2. Hall resistance for two orientations at 330 mK demonstrating that the carrier density is isotropic.

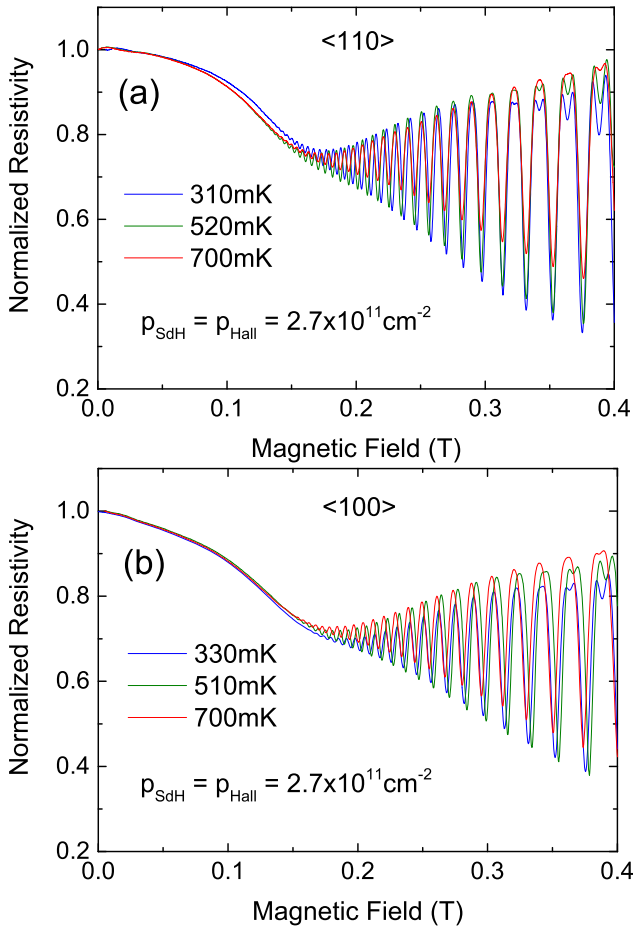

FIG. 3. Low temperature magnetoresistance curves for the two crystallographic orientations (a) ⟨110⟩ and (b) ⟨100⟩, plotted on the same vertical scale to highlight the difference in damping (due to effective mass and scattering parameters).

transport lifetime, the Fermi energy, or the quantum lifetime. As the carrier density is constant, we know that the Fermi energy is also constant, leaving the other three parameters as potential origins of the change in damping.

The effective mass and Dingle ratio may be determined by an iterative solution of Eq. (1), using the temperature dependence of the peak amplitudes of the Shubnikov-de Haas oscillations. This procedure is described in detail elsewhere.[18] Oscillations in the field range up to 0.4 T at temperatures between 0.3 and 2 K were used for the analysis. The peak amplitudes are plotted in Fig. 4, after transformation into the quantities that may be used for solution of Eq. (1). The iterative procedure yields an effective mass of $0.055m_0 \pm 0.005$ for the ⟨110⟩ direction and $0.035m_0 \pm 0.005$ for the ⟨100⟩ direction, and a Dingle ratio of 60 and 70 for the ⟨110⟩ and ⟨100⟩ directions respectively. These values are much lower than previously observed in other studies on lower mobility Ge QW structures (typically 0.065 m_0 and above). From these values, we may then calculate the transport lifetime (40.3 ps and 23.1 ps), the mean free path (11.1 and 10.0 μm), and the quantum lifetime (0.67 ps and 0.33 ps). These key transport parameters are summarized in Table I. For each epi wafer, we performed measurements on large number of Hall bars with surface orientation changing every 45°. As expected, anisotropy was observed only for Hall bars orientated every 45°. In other words, there is no anisotropy for Hall bars orientated at 0°, 90°, 180°, etc. Three devices were measured and fitted for each crystalline direction. The error bars are substantially smaller compared to what is observed as transport anisotropy across different crystal directions.

To summarize the anisotropy between the ⟨110⟩ and ⟨100⟩ directions, in the ⟨110⟩ direction, the transport lifetime and quantum lifetime are larger by a factor of 2, the effective mass is larger by a factor of 1.5, and the mean free path is 10% larger. Intuitively, we would expect carriers with a lower effective mass to have a higher mobility, but the opposite is seen here. This suggests that the intrinsic band structure of the quantum well is not the most important factor when determining the transport properties and the scattering length of carriers. We must therefore consider scattering mechanisms as a potential origin of this anisotropy. As the quantum lifetime is proportional to the sum of all scattering probabilities at all angles, then a change in any scattering mechanism at all will cause the quantum lifetime to vary. However, the transport lifetime is a weighted sum by the scattering angle, such that only large angle scattering events contribute to this parameter.[16] As both quantum and transport lifetimes change, the dominant contribution to the anisotropy is from large angle scattering. Potential large angle scattering includes scattering from ionised impurities inside the 2DHG layer or from the QW interface with the spacer. The structure of the wafer is permeated with the cross-hatching pattern visible on the surface in Fig. 1(c). One potential origin of the anisotropy is therefore increased interfacial scattering in the ⟨100⟩ direction due to carriers intersecting with the cross-hatch at an angle of 45°. However, the periodicity of the crosshatches is ~1–2 μm, but the mean free path along this direction is still substantially longer (10 μm). This leads us to the conclusion that the morphology of the surface is not responsible for the observed anisotropy. Alternatively, impurities within the quantum well may be localised into the cross-hatch regions, causing the degree of impurity scattering to vary with current direction. The Ge QW and SiGe spacer interface scattering is a more likely candidate, given the long mean free path at low temperatures (10 μm) and the low density of unintentional background impurities within the QW (less than 10^{15} cm^{-3} for B and P defined by the detection limit of SIMS measurements). However, it requires further research by high resolution transmission electron microscopy. It is worth noting at this point that the overall dominant scattering mechanism in the quantum transport regime is in fact remote impurity scattering, as evidenced by the very large Dingle ratio (>60) in both transport directions.[19–23] However, scattering of this type (small angle) does not contribute to mobility anisotropy, as discussed earlier. The anisotropy present is clearly observable due to the large mobility in this QW structure, enhanced by biaxial compressive strain. Indeed, the difference in mobility between the two directions is comparable to the highest mobility observed in this system up until only three years ago. It would appear that strain enhances the anisotropy, and if this is the case, then future experiments with varying the strain in the Ge QW ought to provide evidence to support our current explanations and predictions.

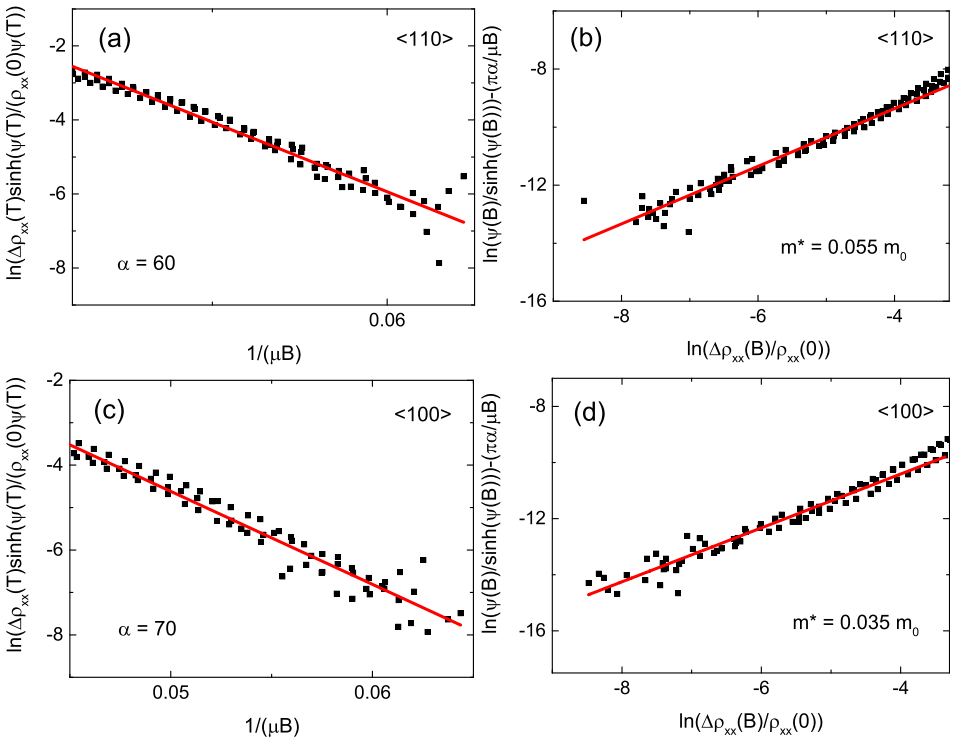

FIG. 4. The effective mass can be calculated from the temperature dependence of the Shubnikov de-Haas peak amplitudes by an iterative process using Eq. (1). The quantities that may be calculated to solve Eq. (1) are plotted for (a), (b) ⟨110⟩ and (c), (d) ⟨100⟩ crystallographic orientations.

TABLE I. Material parameters at a temperature of 0.3 K in two orientations, determined from magnetotransport measurements. The error bars are substantially smaller compared to what is observed as transport anisotropy across different crystal directions.

Crystallographic orientation	Sheet resistivity (Ω/sq.)	Mobility (cm^2/V s)	Carrier density (10^{11} cm^{-2})	Effective mass (m_0)	Dingle ratio	Transport lifetime (ps)	Quantum lifetime (ps)	Mean free path (μm)
⟨110⟩	18.0 ± 0.1	1 288 000 ± 10 000	2.7 ± 0.1	0.055 ± 0.005	60 ± 1	40.3 ± 0.1	0.67 ± 0.01	11.1 ± 0.1
⟨100⟩	20.0 ± 0.1	1 160 000 ± 10 000	2.7 ± 0.1	0.035 ± 0.005	70 ± 1	23.1 ± 0.1	0.33 ± 0.01	10.0 ± 0.1

In summary, the 2DHG carrier density in biaxial strained Ge QW is isotropic at low temperatures, whereas the resistivity of the quantum well exhibits anisotropy. This arises from a 10% increase in hole mobility under a rotation of 45° in the (001) plane from a ⟨100⟩ to a ⟨110⟩ direction. Transport and quantum carrier lifetimes increase by a factor of approximately 2. The effective mass also exhibits anisotropy. However, the direction of the lowest effective mass does not correspond to the highest mobility as is usually assumed. This suggests that the dominant mechanism determining the carrier mobility is scattering from interfaces, impurities, or acoustic phonons and not the intrinsic band structure due to carrier interactions with the lattice. This finding has implications for a very large variety of not only existing, but also future device applications utilising technologically relevant and emerging materials such as SiGe, SiC, GeSn, GeSnSi, and C (Diamond). These findings suggest that electronic device orientation should be carefully chosen to maximise carrier mobility and all dependent device parameters, to increase the uniformity and yield of device arrays or design a new device architecture based on observed anisotropy. These findings also highlight the importance of utilising a device geometry with a well-defined current orientation, i.e., Hall-bar. This is relevant not only for industrial applications, but also for basic materials research where a van der Pauw geometry is commonly used to measure carrier mobility of new materials or structures due to simplicity of device fabrication. We clearly demonstrate the importance of using a Hall bar device geometry for such fundamental measurements. We expect this anisotropy to also be present in 3D bulk materials, but quantification of the effective mass anisotropy is not possible without quantum transport behaviour being present. We would also expect these effects to be enhanced in 1D structures, due to the quantum confinement along a single crystallographic direction and existence of uniaxial strain.

This work was supported by the EPSRC funded Spintronic device physics in Si/Ge Heterostructures, EP/J003263/1 project.

[1]M. V. Fischetti, Z. Ren, P. M. Solomon, M. Yang, and K. Rim, J. Appl. Phys. **94**, 1079 (2003).
[2]R. H. Kingston, *Semiconductor Surface Physics* (University of Pennsylvania Press, 1957).
[3]F. S. Ham and D. C. Mattis, IBM J. Res. Dev. **4**, 143 (1960).
[4]R. F. Pierret and C. T. Sah, Solid-State Electron. **11**, 279 (1968).
[5]V. Aubry-Fortuna and P. Dollfus, J. Appl. Phys. **108**, 123706 (2010).
[6]Y. I. Gorkun, V. S. Lysenko, V. G. Litovchenko, and V. A. Novominskii, Phys. Status Solidi A **3**, K281 (1970).
[7]S. Dissanayake, Y. Zhao, S. Sugahara, M. Takenaka, and S. Takagi, J. Appl. Phys. **109**, 033709 (2011).
[8]A. H. A. Hassan, R. J. H. Morris, O. A. Mironov, R. Beanland, D. Walker, S. Huband, A. Dobbie, M. Myronov, and D. R. Leadley, Appl. Phys. Lett. **104**, 132108 (2014).
[9]M. Failla, M. Myronov, C. Morrison, D. R. Leadley, and J. Lloyd-Hughes, Phys. Rev. B **92**, 045303 (2015).

[10]J. Foronda, C. Morrison, J. E. Halpin, S. D. Rhead, and M. Myronov, J. Phys.: Condens. Matter **27**, 022201 (2014).
[11]C. Morrison, P. Wiśniewski, S. D. Rhead, J. Foronda, D. R. Leadley, and M. Myronov, Appl. Phys. Lett. **105**, 182401 (2014).
[12]Q. Shi, M. A. Zudov, C. Morrison, and M. Myronov, Phys. Rev. B **91**, 201301 (2015).
[13]M. Myronov, C. Morrison, J. Halpin, S. Rhead, C. Casteleiro, J. Foronda, V. A. Shah, and D. Leadley, Jpn. J. Appl. Phys., Part 1 **53**, 04EH02 (2014).
[14]M. Myronov, C. Morrison, J. Halpin, S. Rhead, J. Foronda, and D. Leadley, Solid-State Electron. **110**, 35 (2015).
[15]A. Dobbie, M. Myronov, R. J. H. Morris, A. H A. Hassan, M. J. Prest, V. A. Shah, E. H. C. Parker, T. E. Whall, and D. R. Leadley, Appl. Phys. Lett. **101**, 172108 (2012).
[16]P. Coleridge, R. Stoner, and R. Fletcher, Phys. Rev. B **39**, 1120 (1989).
[17]A. Isihara and L. Smrcka, J. Phys. C: Solid State Phys. **19**, 6777 (1986).
[18]Y. F. Komnik, V. V. Andrievskii, I. B. Berkutov, S. S. Kryachko, M. Myronov, and T. E. Whall, Low Temp. Phys. **26**, 609 (2000).
[19]B. Rössner, D. Chrastina, G. Isella, and H. von Känel, Appl. Phys. Lett. **84**, 3058 (2004).
[20]B. Rößner, G. Isella, and H. V. Känel, Appl. Phys. Lett. **82**, 754 (2003).
[21]K. Sawano, Y. Kunishi, Y. Shiraki, K. Toyama, T. Okamoto, N. Usami, and K. Nakagawa, Appl. Phys. Lett. **89**, 162103 (2006).
[22]A. Gold, Phys. Rev. B **38**, 10798 (1988).
[23]T. Irisawa, M. Myronov, O. A. Mironov, E. H. C. Parker, K. Nakagawa, M. Murata, S. Koh, and Y. Shiraki, Appl. Phys. Lett. **82**, 1425 (2003).
[24]M. Failla, J. Keller, G. Scalari, C. Maissen, J. Faist, C. Reichl, W. Wegscheider, O. J. Newell, D. R. Leadley, M. Myronov, and J. Lloyd-Hughes, New J. Phys. **18**(11), 113036 (2016).